A Zero-Power Ubiquitous Wireless Liquid-Level Sensor Based on Microfluidic-Integrated Microstrip Antenna

Liang Zhu¹⁰, Graduate Student Member, IEEE, Nabeel Alsaab, Mark Ming-Cheng Cheng, Member, IEEE, and Pai-Yen Chen¹⁰, Senior Member, IEEE

Abstract-Harmonic transponder sensors, receiving radiofrequency (RF) signal and converting it to a modulated second harmonic, have been demonstrated to be effective for signal interrogation in environments with strong clutters. Here, we propose a compact dual-resonance microstrip antenna consisting of an elliptical patch loaded with shorting pins. Such an antenna utilizes the TM_{e110} resonant mode to intercept the perpendicularly-polarized fundamental tone (2.86 GHz) and uses the TM_{o110} resonant mode to retransmits the parallelly-polarized second harmonic (5.72 GHz). Moreover, we have developed a harmonic-based wireless liquid sensor comprising the proposed antenna and a micromachined liquid channel. Our measurement results show that even in the noisy environment, the second harmonic strength can precisely indicate the dielectric property of liquid filled in the microfluidic tank (e.g., acetone-water mixtures with various concentrations). However, a similar setup without frequency and polarization modulations (i.e., linear and passive backscatter tag) fails to provide a sensitive and quantitative measurement of liquid property. The proposed low-profile dual-resonance antenna with sensing capability will pave the way for the development of harmonic sensors and nonlinear radio-frequency identification (RFID) tags.

Index Terms—Harmonic sensors, antenna sensors, clutter, electromagnetic interreferences, low-noise passive wireless sensors, dual-band antennas, elliptical patch antennas.

I. Introduction

Compact and zero-power wireless sensors have been the subject of intense research in the past few years because of their practical uses in many engineering applications, including Internet-of-Things (IoTs), industrial 4.0, smart cities, wireless healthcare and environmental monitoring, to name a name [1]–[3]. In most passive wireless sensor systems, a reader transmits a continuous-wave (CW) RF signal to power the tag and receives the backscattered signal, which is generally modulated by a mounted physical or chemical sensor varying the antenna's input impedance [4]–[7]. In these systems, the CW signal that powers up the passive

Manuscript received February 7, 2020; revised April 24, 2020 and June 8, 2020; accepted June 18, 2020. Date of publication June 23, 2020; date of current version August 26, 2020. (Corresponding author: Pai-Yen Chen.)

Liang Zhu, Nabeel Alsaab, and Pai-Yen Chen are with the Department of Electrical and Computer Engineering, University of Illinois, Chicago, IL 60607 USA (e-mail: pychen@uic.edu).

Mark Ming-Cheng Cheng is with the Department of Electrical and Computer Engineering, University of Alabama, Tuscaloosa, AL 35487 USA. Digital Object Identifier 10.1109/JRFID.2020.3004351

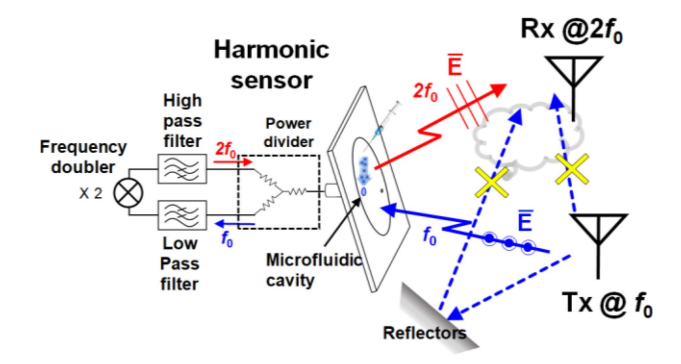


Fig. 1. Schematics of a compact harmonic transponder sensor (or harmonic sensor) based on the microfluidic-integrated, dual-resonance elliptical patch antenna connected to the diplexer and frequency doubler. The sensor can receive and retransmit RF signals with orthogonal frequencies and polarizations for avoiding clutter and cross talk.

tags is inevitably coupled to the receiver, presenting a strong self-interference that poses a major challenge to the reader's receiver design. Moreover, these systems are also vulnerable to surrounding reflections and noises, which limits their practical applications in the noisy indoor environment full of echos, clutters and crosstalks [8]-[10]. Very recently, nonlinear harmonic-based tracking and sensing techniques have been gained increasing popularity because of their capability to eliminate the crosstalk between the reader's transceiver and receiver antennas (R_x and T_x), as well as the unwanted clutters and echoes from a noisy environment, as schematically shown in Fig. 1 [11]-[14]. Unlike traditional passive wireless sensor systems, of which reader and sensor working at the same frequency [15]-[17], the passive harmonic sensor system has a nonlinear tag or harmonic transponder that receives a fundamental tone, modulating the received RF signal, and retransmitting a high/sub-harmonic tone (e.g., second harmonic) to the reader (Fig. 1) [18], [19]. Thanks to the frequency orthogonality between the launched and backscattered signals, the harmonic sensor system can remarkably suppress electromagnetic interferences, such as crosstalk and clutter [20], [21]. According to this principle, Huang et al. have demonstrated a passive harmonic sensor for liquid sensing in healthcare applications. This technique is based on the received signal strength indicator (RSSI) data in the harmonic band and the UHF frequency-hopping spread spectrum (FHSS)

analysis [22]. In particular, this technique is useful for interrogating electrically-small sensors/tags, which typically suffer from electromagnetic interferences in rich-scattering environments, such as the dense urban and indoor areas.

Although the harmonics-based passive wireless sensor systems have advantages in terms of high signal-to-noise ratio (SNR) and longer wireless interrogation distance, the sensor/tag usually has two antennas for receiving the fundamental tone and retransmitting high/sub-harmonic frequencies [23], [24]. This, in turn, increases the complexity in minimization and integration of the sensor. Attempting to develop compact and low-profile harmonic sensors, we proposed here a dual-resonance elliptical microstrip patch antenna, which enables a single feedline to excite the first even mode (TM_{e110}) at the fundamental frequency (f_0) and the first odd mode (TM_{o110}) at the second-harmonic frequency $(2f_0)$, as depicted in Fig. 1. Moreover, these two modes have different polarizations perpendicular to each other, which further reduces one stage of interference. This singlefeed microstrip antenna can be connected to a diplexer and a frequency doubler for making a compact harmonic transponder. In addition to the device miniaturization enabled by hybridization of the tag's receiving and transmitting antennas $(R'_{x} \text{ and } T'_{x})$, the proposed microstrip antenna can be readily mounted with sensing elements to form a harmonic sensor. For example, if a fluidic channel is suitably loaded onto the elliptical patch, the resonance frequency of the TM_{o110} mode can be sensitively tuned, whereas the resonance frequency of the TM_{e110} remains unchanged. In this manner, the sensor/tag always receives the same input fundamental tone, while the output second harmonic received by the reader has a magnitude tuned by the dielectric property or volume of the liquid under test.

This paper is organized as follows. In Section II, we will derive the analytical model for computing resonant modes and field distributions of the proposed dual-resonance microstrip antenna. In Section III, we will report the experimental results for the proposed antenna, in terms of impedance matching and radiation characteristics. We will propose a shorting-pin modal tuning method to decouple the TM_{e210} and TM_{o110} modes, which could have similar resonance frequencies. We will also demonstrate a fully-passive harmonic sensor comprising the proposed compact microstrip antenna mounted with a fluidic channel, for practical liquid and humidity monitoring in noisy environments. Finally, we will draw a short conclusion.

II. THEORETICAL MODELING OF DUAL-BAND ELLIPTICAL PATCH ANTENNA

Fig. 1 depicts the geometry of the proposed elliptical microstrip antenna with the major semi-axis length a and the minor semi-axis length b. The elliptical patch layer is separated from the ground plane by the FR4 substrate with thickness d=1.5 mm, relative permittivity $\varepsilon_r=4.25$, and loss tangent $\delta=0.015$. The resonant modes of the elliptical antenna can be computed by using the cavity model with proper boundary conditions [25], [26]. The perfect electric conductor (PEC) boundary condition is applied at the top and

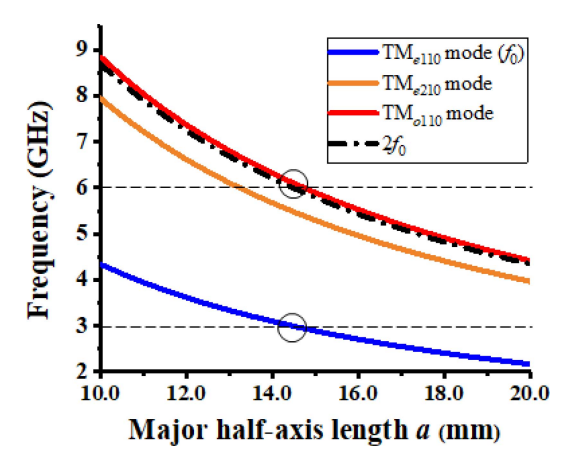


Fig. 2. Resonance frequencies of the proposed elliptical patch antenna for different operating modes.

bottom surfaces, and the perfect magnetic conductor (PMC) is assumed on sidewalls. In this case, Maxwell's equations reduce to the following set of equations in elliptical coordinates (ξ, η) , where $\xi \in [0, \infty]$ and $\eta \in [0, 2\pi]$ [27], [28]:

$$\frac{1}{c^2(\cosh^2\xi - \cos^2\eta)} \left(\frac{\partial^2 E_z}{\partial \xi^2} + \frac{\partial^2 E_z}{\partial \eta^2}\right) + k^2 E_z = 0,$$

$$H_{\xi} = j \frac{1}{\omega\mu c \left(\cosh^2\xi - \cos^2\eta\right)^{1/2}} \frac{\partial E_z}{\partial \eta},$$

$$H_{\eta} = -j \frac{1}{\omega\mu c \left(\cosh^2\xi - \cos^2\eta\right)^{1/2}} \frac{\partial E_z}{\partial \xi},$$

$$H_z = 0, E_{\xi} = 0, \text{ and } E_{\eta} = 0.$$
(1)

The electric fields inside this cavity can be expanded in terms of elliptical wave functions as:

$$E_{e,z}(\xi,\eta) = \sum_{n=0}^{n=\infty} M_{e,n}^{(1)}(\xi,q) C_{e,n}(\eta,q),$$

$$E_{o,z}(\xi,\eta) = \sum_{n=1}^{n=\infty} M_{o,n}^{(1)}(\xi,q) S_{e,n}(\eta,q),$$
(2)

where $q=c^2k^2/4$, $k=\omega\sqrt{\varepsilon_r\varepsilon_0\mu_0}$, $c=\sqrt{a^2-b^2}$, ε_0 and μ_0 are free space permittivity and permeability, $M_{e,n}^{(1)}(\xi,q)$ and $M_{o,n}^{(1)}(\xi,q)$ are respectively the even and odd radial Mathieu function of the first kind, n is the order of the angular Mathieu functions $C_{e,n}(\eta,q)$ and $S_{e,n}(\eta,q)$, which determine the azimuthal variation along η , [29], [30]. By matching the boundary conditions at the magnetic sidewall $\xi=\xi_0$, the transcendental equations are given by:

$$M'_{e,n}^{(1)}(\xi_0,q) = 0$$
 for *n*-th even mode $M'_{o,n}^{(1)}(\xi_0,q) = 0$ for *n*-th odd mode (3)

By solving the above transcendental equation (Eq. (3)), if ξ_0 = 0.497 (b/a = 0.46), the first even mode TM_{e110} and the first odd mode TM_{o110} mode can be respectively excited at f_0 and $2f_0$, as can be seen in Fig. 2. When designing an elliptical antenna for harmonic transponders, one needs to first decide the major semi-axis length a, in order to obtain resonance at

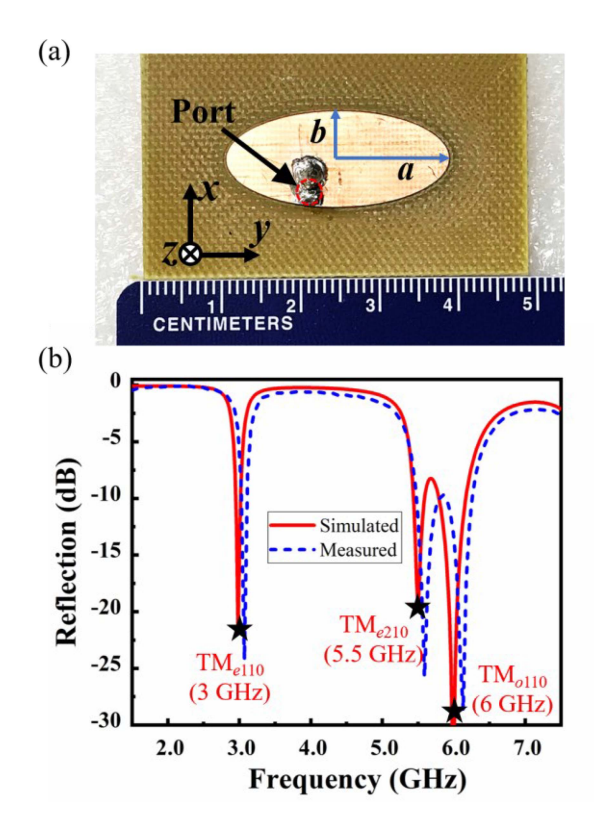


Fig. 3. (a) Photograph of the dual-resonance elliptical patch antenna. (b) The simulated and measured reflection coefficient (S_{11}) of the antenna in (a); here, solid and dash lines represent the simulated and measured results, respectively, and stars represent analytical results obtained from Eq. (3).

 f_0 (TM_{e110} mode). Then, minor semi-axis length b is automatically determined, as b=0.46a, resulting in resonance at $2f_0$.

III. EXPERIMENTAL RESULTS

A. Dual-Resonant Elliptical Microstrip Antenna Without Shorting Pins

We have fabricated the proposed elliptical-patch microstrip antenna using printed-circuit board (PCB) technique, with FR4 substrate and copper (Cu) microstrips. Fig. 3(a) reports the fabricated dual-resonance elliptical patch antenna; here, important design parameters are a = 14.4 mm and b =6.336 mm, and a 50 ohms coaxial cable feed is positioned at x = -3 mm and y = -3.5 mm. By suitably positioning the feed point, one may be able to simultaneously excite the TM_{e110} and TM_{o110} modes, which yield orthogonal, linearly-polarized radiation in the far zone. Fig. 3(b) reports the simulated [31] and measured reflection coefficients (S_{11}) versus frequency for the microstrip antenna in Fig. 3(a). It is evident that the measured and simulation results are in a good agreement. Noticeable dips can be found at 3 GHz and at 6 GHz, confirming the dual-resonance behaviors of the proposed structure. Moreover, good impedance matching is obtained, with the measured -10 dB impedance bandwidth of 80 MHz in the first band (center frequency is 3.07 GHz) and of 350 MHz in the second band (center frequency is 6.13 GHz). These values are closed to the simulation results, which are 70 MHz and 380 MHz.

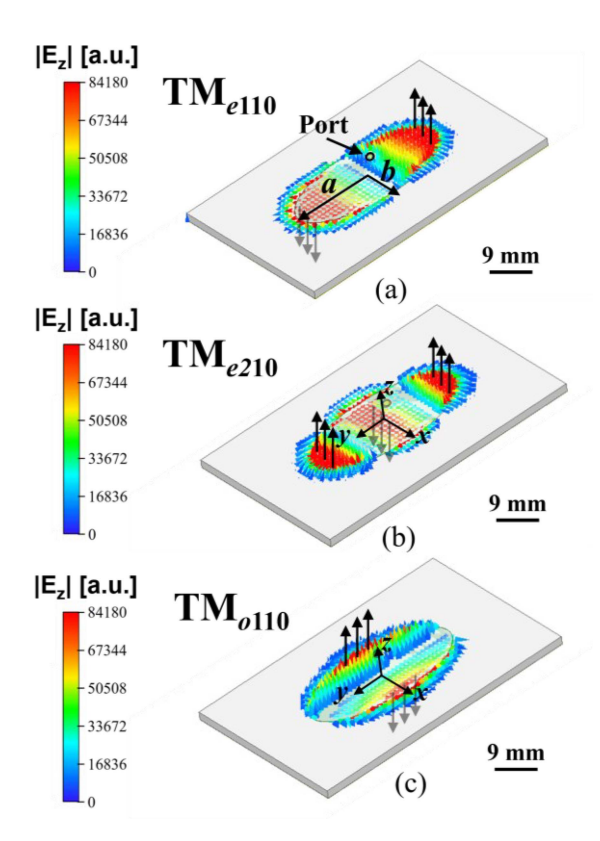


Fig. 4. Simulated snapshots of electric field (E_z) distributions for (a) the TM_{e110} mode (3 GHz), (b) the TM_{e210} mode (5.5 GHz) and (c) the TM_{o110} mode (6 GHz) of the single-feed, dual-resonance elliptical microstrip antennas in Fig. 3.

Figs. 4(a) and 4(c) report the simulation results for snapshots of electric field distributions of the TM_{e110} and TM_{o110} modes, respectively. The field profiles agree well with what predicted by the cavity model. We note that the TM_{e210} mode is also excited in the proximity of the TM_{o110} mode, as highlighted in Figs. 2 and 3(b). Such a higher-order even mode needs to be suppressed or red/blue-shifted (down/up-shifted), in order to avoid the modal coupling. A simple, but yet effective, solution using the shorting-pin loads to redshift the TM_{e210} mode will be discussed in the next section.

Fig. 5 reports the simulated and measured radiation patterns of this antenna on the E- and H-planes at the two resonance frequencies. The E- and H-planes for the $TM_{e110}(TM_{o110})$ modes are y-z and x-z (x-z and y-z) planes, respectively. The broadside radiation pattern was measured for both resonant modes, in good agreement with the simulation results. At 3 GHz (TM_{e110} mode), the antenna exhibits a maximum realized gain of 2.66 dBi, with a half-power beamwidth (HPBW) of 92° on the E-plane and a HPBW of 106° on H-plane. At 6 GHz (TM_{o110} mode), the antenna exhibits a maximum gain of 4.84 dBi, with a HPBW of 84° (66°) on the E-plane (H-plane). Moreover, a high co-polarization was measured, with a cross-polarization less than -20 dB (-10 dB) on the E-plane (H-plane). Due to relatively high dielectric and conduction losses of the substrate used here, the measured radiation efficiencies are 45% at 3 GHz and 83% at 6 GHz. It is known that the radiation efficiency of microstrip antennas generally decreases when the substrate thickness or permittivity is

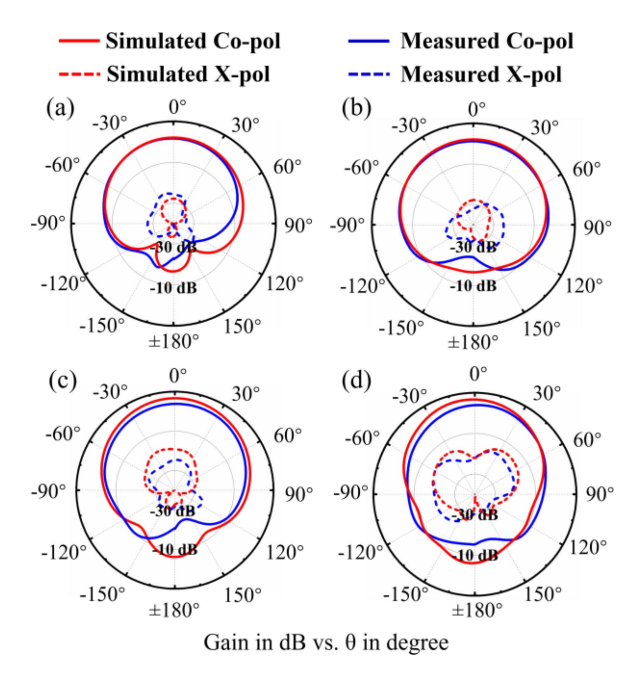


Fig. 5. Simulated and measured radiation patterns of the dual-resonance elliptical patch antenna in Fig. 3: (a) and (b) are the radiation patterns on the E-plane (*y-z* plane) and the H-plane (*x-z* plane) at 3 GHz; (c) and (d) are the radiation patterns on the E-plane (*x-z* plane) and the H-plane (*y-z* plane) at 6 GHz.

increased because of loss to surface waves. On the other hand, the radiation efficiency may also decrease when the substrate becomes thinner due to the more severe conduction and dielectric loss in thinner substrate [32], [33]. This may explain why the radiation efficiency in the 3 GHz band is lower than that in the 6 GHz band, simply because the substrate thickness relative to the operating wavelength decreases, thus resulting in relatively high conduction and dielectric loss. The radiation efficiency can be improved by using the high-quality PCB substrate with a low loss tangent.

B. Elliptical Microstrip Antenna Loaded With Shorting Pins

Even though the above dual-resonance elliptical patch antenna has good impedance matching and radiation properties at the frequencies of interest, the spectral overlap between the TM_{o110} and TM_{e210} modes (see Figs. 2 and 3(b)) must be mitigated. It is not possible to decouple the TM_{e210} and TM_{o110} modes by simply varying the ellipse or dimension of the elliptical patch. Here, we propose a shorting-pin method to decouple these two modes. Inserting shorting pin (e.g., through via) inside the cavity could perturb the current path induced on the microstrip patch antenna, which has been used for making dual-band patch antennas [34]–[36] and for miniaturizing the size of patch antenna [37]-[39]. Fig. 6(a) shows the proposed design, with two shorting pins placed on the y (major)-axis of the elliptical patch. The dimensions of this dual-resonance elliptical patch are slightly modified to a = 19.5 mm and b = 6.63 mm, in order to fix resonance frequencies. We have swept the separation distance between the two shorting pins, g, along the y-axis. The simulated resonance frequencies for TM_{e110} , TM_{e210} and TM_{o110} modes are shown in Fig. 6(b). It is clearly seen that increasing the distance between two

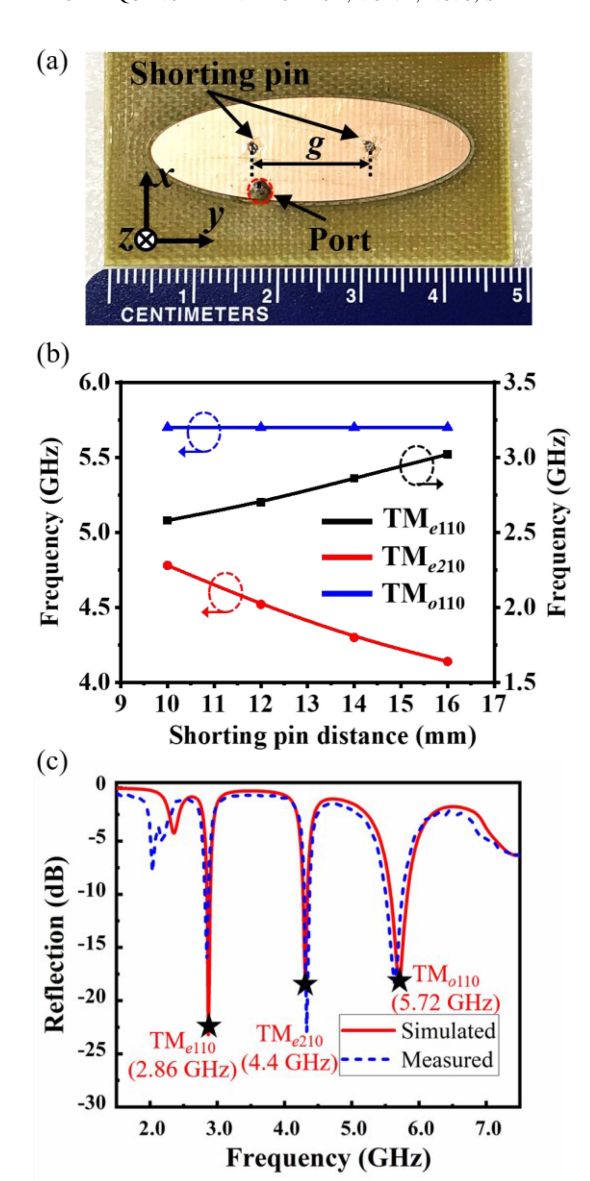


Fig. 6. (a) Photograph of the dual-resonance elliptical microstrip antenna loaded with two shorting pins. (b) Simulated resonance frequencies of the proposed antenna with different separation distance *g* between two shorting pins. (c) Simulated and measured reflection coefficients of the antenna in (a).

shorting pins, the resonance frequency of TM_{e110} mode is upshifted from 2.58 GHz to 3.02 GHz, while that of the TM₀₁₁₀ mode is almost unchanged. More interestingly, the resonance frequency of the TM_{e210} mode is downshifted from 4.78 GHz to 4.14 GHz, such that the TM_{0110} and TM_{e210} can be separated from each other. The existence of shorting pins along y (major)-axis only affect electrical field distributions of the TM_{e110} and TM_{e210} modes (see Fig. 4), leading to the resonance frequency offsets, and has no effect on the TM_{o110} mode. Increasing the separation distance between the two shorting pins would shorten the current path of TM_{e110} mode, while enlarging the current path of TM_{e210} . As a result, adding the shorting-pins will upshift the TM_{e110} mode, while downshifting the TM_{e210} in the spectrum. On the other hand, since the electrical field of the TM_{o110} mode is null on the plane of x = 0 (see Fig. 4(c)), it implies that the two shorting

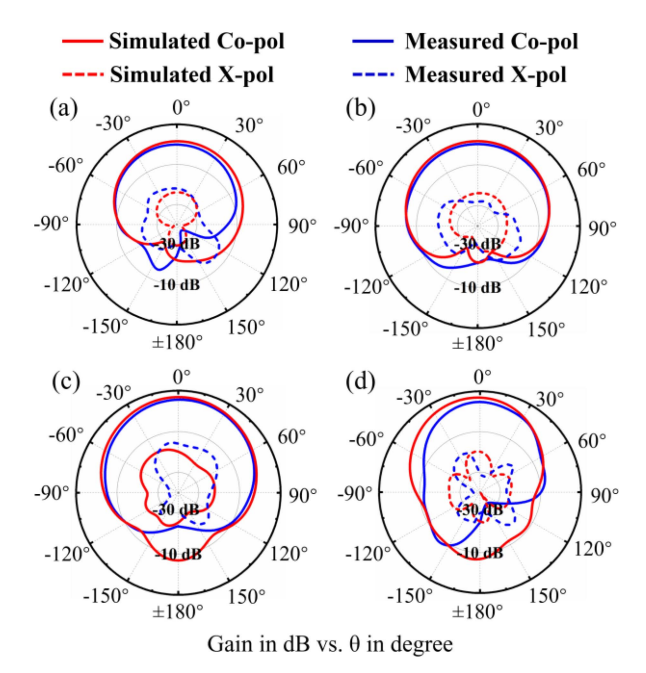


Fig. 7. Simulated and measured radiation patterns of the dual-resonance antenna in Fig. 6: (a) and (b) are the radiation patterns on the E-plane (y-z plane) and the H-plane (x-z plane) at 2.86 GHz; (c) and (d) are the radiation patterns on the E-plane (x-z plane) and the H-plane (y-z plane) at 5.72 GHz.

pins have no effect on field distribution and center frequency of the TM_{o110} mode.

According to the results in Fig. 6(b), we have redesigned the elliptical patch antenna that has decoupled TM_{o110} and TM_{e210} modes; here, the important design parameters are: a = 19.5 mm, b = 6.63 mm, the shorting-pin radius $r_{pin} = 0.4$ mm, and g = 14 mm. Figs. 6(a) and 6(c) report the fabricated microstrip antenna and its reflection coefficients. It is evident that loading the shorting pins can effectively isolate the TM_{e210} mode and TM_{o110} mode. However, a dual resonance ($f_0 = 2.86$ GHz and $2f_0 = 5.72$ GHz) is still obtained in the shorting-pin-loaded elliptical microstrip antenna. The measured -10 dB impedance bandwidth is 50 MHz in the first band (the center frequency is 2.845 GHz) and is 270 MHz in the second band (the center frequency is 5.65 GHz), which are consistent with the simulation results. Fig. 7 reports the radiation pattern of this antenna on the E- and H-planes at 2.86 GHz and 5.72 GHz; here, the definition of E- and H-planes are the same as Fig. 5. It is observed that adding the shorting pins does not affect the radiation patterns and co-/cross-polarization of the elliptical patch antenna. At 2.86 GHz, the antenna exhibits a maximum realized gain of 1.55 dBi, with a half-power beamwidth (HPBW) of 85° on the E-plane and a HPBW of 120° on the H-plane. At 5.72 GHz, the antenna exhibits a maximum gain of 6.7 dBi, with a HPBW of 80° (55°) on the E-plane (H-plane). The measured cross-polarization radiation pattern is less than -15 dB (-15 dB) on the E-plane (H-plane). The radiation efficiency is measured to be 43% at 2.86 GHz and 83% at 5.72 GHz, which are comparable to the radiation efficiency of the unloaded elliptical patch antenna in Fig. 3. We should note that inserting the shorting into the cavity can be considered as a resistive perturbation for the

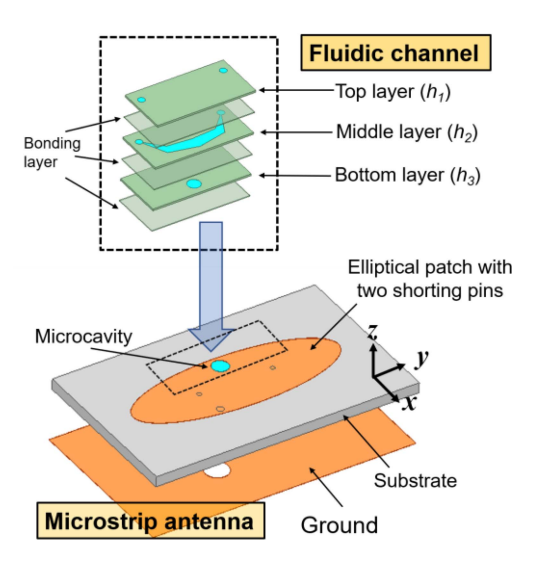


Fig. 8. Schematic of the integrated harmonic sensor consisting of the dualband elliptical patch antenna and an acrylic based fluidic channel.

 TM_{e110} mode (2.86 GHz), which may increase the conduction loss and reduce the radiation efficiency of such mode. On the other hand, the position of the shorting-pin is located in the null-field region for the TM_{o110} mode (5.72 GHz), as can be seen in Fig. 4, thereby not affecting the radiation efficiency of the first odd mode. This compact dual-band microstrip antenna with a good tunability may benefit the design of harmonic transponders used in various applications.

IV. PRACTICAL WIRELESS LIQUID MONITORING

A. Harmonic Transponder Based on the Dual-Resonance Elliptical Patch Antenna

We have developed a harmonic sensor that integrates the dual-resonance microstrip antenna in Fig. 6(a) and a fluidic channel, as schematically shown in Fig. 8. The liquid tank with radius $r_{tank} = 1.5$ mm is located at x = 5 mm and y = 0 mm and the parameters of the loaded fluidic channel is L = 25 mm, W = 12 mm with height $h_1 = 1$ mm, $h_2 = 1$ mm and $h_3 = 0.1$ mm for three layers, respectively. It should be emphasized that at the center of the microfluidic cavity, the TM₀₁₁₀ resonant mode exhibits a peak electric field, whereas the TM_{e110} resonant mode has null electric field. According to the perturbation theory [40], [41], when the dielectric property of the fluidic channel is varied, the resonance frequency of the TM_{o110} mode (at $2f_0$) may experience a relevant shift, owning to strong electric fields localized in the liquid reservoir region (Fig. 4(a)). On the other hand, the TM_{e110} mode (at f_0) remains unchanged due to null electric field in the region where the liquid reservoir is located (Fig. 4(c)). Fig. 9 shows the photography of the fabricated harmonic sensor integrated with fluidic channel with two liquid tubes guiding medium in and out, respectively.

Fig. 10 reports the simulated and measured reflection coefficients for such an antenna sensor, which exhibits dominant TM_{e110} , TM_{e210} and TM_{o110} modes at 2.86 GHz, 4.4 GHz, and 5.76 GHz, respectively. The existence of the fluidic channel would shift slightly the peak frequency of

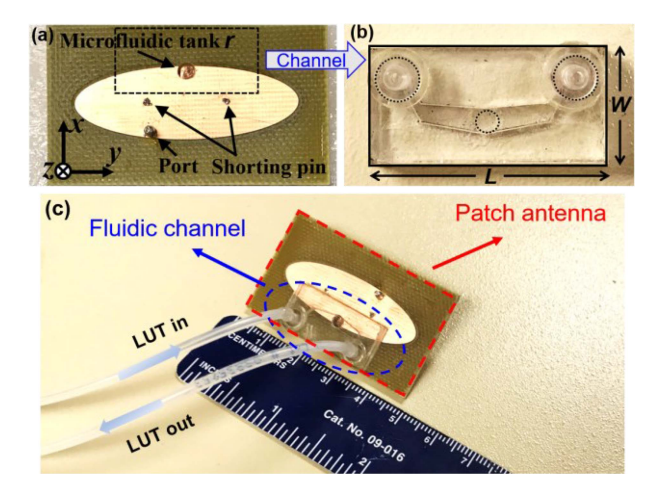


Fig. 9. Photograph of (a) the dual-resonance elliptical patch antenna (top view), (b) the fluidic channel (top view), and (c) the integrated harmonic sensor (prospective view).

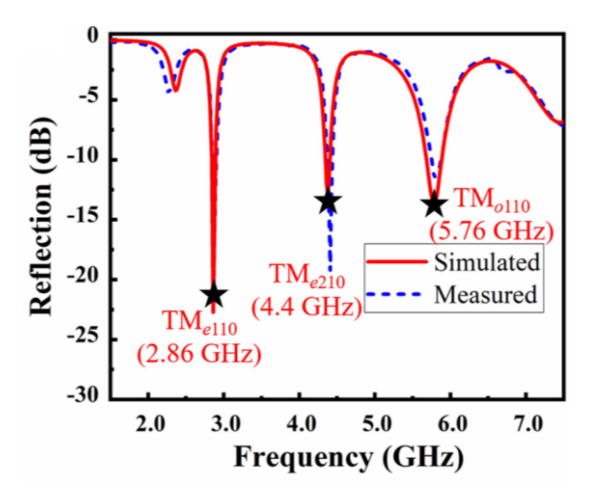
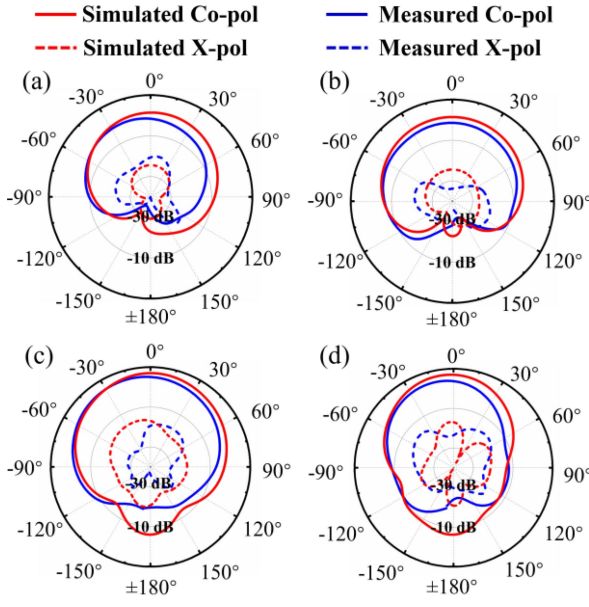


Fig. 10. The simulated and measured reflection coefficient (S_{11}) of the antenna in Fig. 9.

the TM_{o110} mode from 5.72 to 5.76 GHz. Nevertheless, this mode still has a sufficiently broad bandwidth to accommodate the second-harmonic signal. Fig. 11 reports the simulated and measured radiation patterns of the antenna on the E- and Hplanes at the 2.86 GHz and 5.76 GHz, showing quite similar broadside radiation properties as those of the shorting-pinsloaded elliptical patch antenna without fluidic channel (Fig. 7). At 2.86 GHz, this antenna exhibits a maximum realized gain of 0.7 dBi, with a half-power beamwidth (HPBW) of 85° on the E-plane and a HPBW of 110° on H-plane. When compared to the realized gain of the antenna without fluidic channel (1.55 dBi (Fig. 7)), the realized gain is slightly decreased due to errors in fabrication and package. At 5.76 GHz, this antenna exhibits a maximum gain of 6.5 dBi, with a HPBW of 90° (50°) on the E-plane (H-plane). The measured crosspolarization radiation pattern is less than -20 dB (-15 dB)on the E-plane (H-plane).

B. Binary Liquid Mixture Measurement

In this section, the harmonic sensor in Fig. 9 will be used for the practical wireless monitoring of density and dielectric



Gain in dB vs. θ in degree

Fig. 11. Simulated and measured radiation patterns of the dual-resonance elliptical patch antenna in Fig. 9: (a) and (b) are the radiation patterns on E- and H-planes at 2.86 GHz; (c) and (d) are similar to (a) and (b), but at 5.76 GHz. Here, the definitions of E- and H-planes are the same as Fig. 7.

TABLE I
COMPLEX PERMITTIVITIES OF DIFFERENT ACETONE-WATER MIXTURES

| Mixtures | 0 % | 20% | 40% | 60% | 80% | 100 % |
|-------------------|-----------|-----|------|-----|-----|---------|
| | (acetone) | | | | | (water) |
| ε'_r | 20.7 | 25 | 35 | 45 | 66 | 80 |
| ε''_r | 0.5 | 1 | 1.65 | 2.5 | 4.3 | 6 |

constant of acetone-water mixtures. For this purpose, acetone-water mixtures at various concentrations were prepared and their complex-valued effective permittivities are summarized in Table I. Such mixtures' effective relative permittivity ε_r can be computed by the dielectric mixing formula [42], [43], given by:

$$\varepsilon_{r} = \varepsilon_{acetone} \left[\frac{(2\varepsilon_{acetone} + \varepsilon_{water}) + 2V_{f}(\varepsilon_{water} - \varepsilon_{acetone})}{(2\varepsilon_{acetone} + \varepsilon_{water}) - V_{f}(\varepsilon_{water} - \varepsilon_{acetone})} \right]$$
(4)

where ε_{water} [43] and $\varepsilon_{acetone}$ [44] are the complex permittivities of water and acetone, respectively, and V_f is the volume fraction of water in the mixture. Fig. 12 reports the measured reflection coefficients (S₁₁) versus frequency for different acetone-water mixtures. The results in Fig. 12 show that increasing the dielectric constant of the liquid mixture (or, effectively, lowering the volume ratio of acetone to water) will shift the center frequency of TM_{o110} mode from 5.64 GHz to 5.16 GHz. However, the center frequency of TM_{e110} mode is rather unchanged (\sim 2.86 GHz). According to the above results, Fig. 13 summaries the measured resonance frequency shifts of TM_{e110} and TM_{o110} modes, under different volume fractions of water. It is clearly seen that the proposed harmonic sensor shows good sensitivity and linearity in measuring the water (or acetone) concentrations, and the agreement between

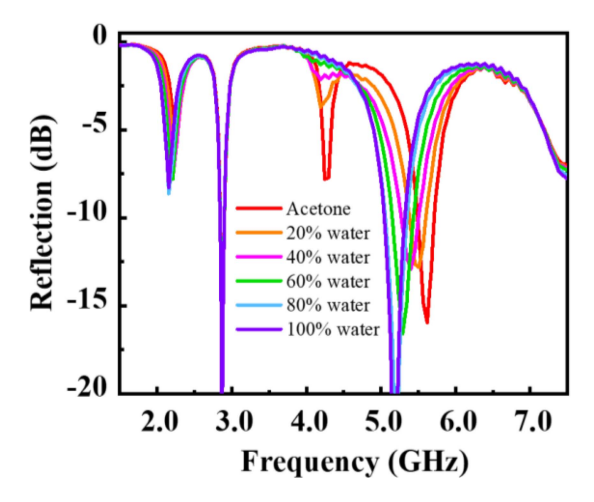


Fig. 12. Measured reflection coefficients of the harmonic sensor which comprises the microstrip antenna in Fig. 9, loaded with acetone/water mixtures at various concentrations.

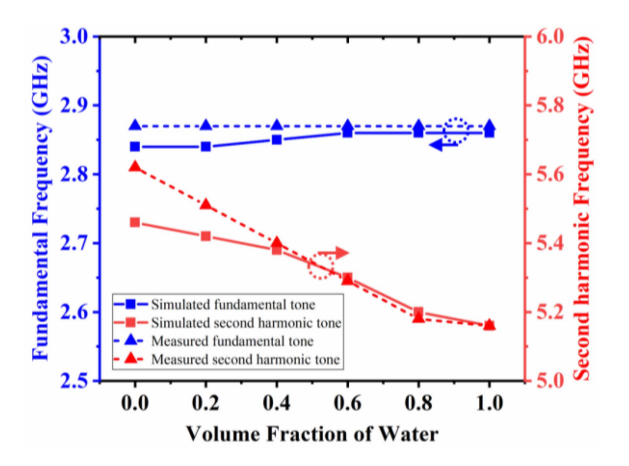


Fig. 13. Simulated and measured frequency responses of the two operating modes for the dual-resonance elliptical patch antenna in Fig. 9.

measurement and simulation results are remarkably good. We have also measured the realized gain of the elliptical patch antenna as a function of volume fraction of water (in units of percentage) at the operating frequencies, and results are reported in Fig. 14. The small difference between the simulated and experimental results could be due to errors in the assembly and fabrication processes, or variations of the FR4 substrate's permittivity. Apparently, it can be seen that the realized gain (G_2) at 5.72 GHz decreases dramatically from 5.8 dBi to -0.7 dBi, as the type of liquid is varied from acetone (0 %), acetone-water mixture (20 %-80 %), to water (100 %), whereas the realized gain (G_1) at 2.86 GHz is, however, fixed to 1.33 dBi. Such results suggest that the input RF signal has a fixed strength, whereas the output second harmonic can be detuned by the density of the liquid mixture.

Next, we consider a fully-passive harmonic sensor prototype made of the microfluid-integrated, dual-band elliptical patch antenna in Fig. 9, connected to a diplexer [45] and a frequency doubler [46]. In our measurements, the bistatic configuration was used for telemetry (see Fig. 15(a)). Firstly, the harmonic sensor was measured inside the noise-free anechoic chamber,

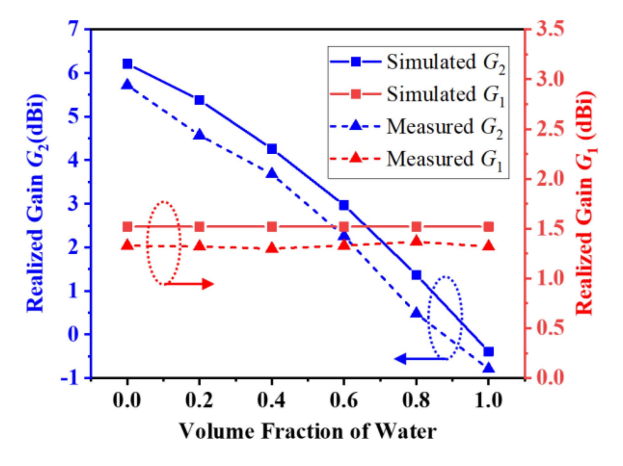


Fig. 14. The simulated and measured realized gain of the dual-resonance harmonic sensor at 2.86 GHz (G_1) and 5.72 GHz (G_2) .

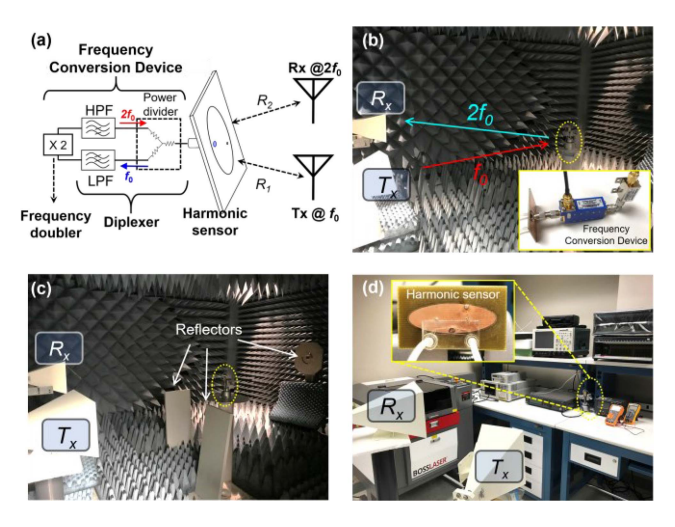


Fig. 15. Measurement setup for characterization of the nonlinear harmonic sensor and the linear backscatter sensor. (a) Block diagram of the bistatic interrogation setup with the background consisting of (b) no reflector, (c) a few reflectors inside the anechoic chamber room, and (d) multiple reflectors of different kinds in a noisy indoor environment.

which remove effects of echoes, clutters, and multipath reflections, as shown in Fig. 15(b). Afterward, metal reflectors were intentionally placed in the proximity of the harmonic sensor, in order to test its immunity to clutter and echo noises as shown in Fig. 15(c). In Fig. 15(d), we repeat our measurement in a noisy indoor environment that is full of clutters, echoes and electromagnetic interferences. In our setups, the transceiver (T_x) launched a CW fundamental tone to the harmonic sensor. The backscattered second harmonic, whose strength depends on the density of dielectric constant of the liquid mixture inside the fluidic channel, was recorded by the receiver (R_x) . According to the Friis' transmission equation [47], the ratio of the power of second harmonic received by R_x to the RF power transmitted by T_x is given by:

$$\frac{P_r}{P_t} = \left(\frac{\lambda_0}{4\pi R_1}\right)^2 \left(\frac{\lambda_0/2}{4\pi R_2}\right)^2 \frac{G_1 G_2 G_T G_R}{L_{\text{SVS}}}$$
(5)

where G_T and G_R are the antenna gain of T_x and R_x , G_1 and G_2 are respectively the gain of the receiving (f_0) and re-transmitting $(2f_0)$ modes of the harmonic sensor, R_1 is

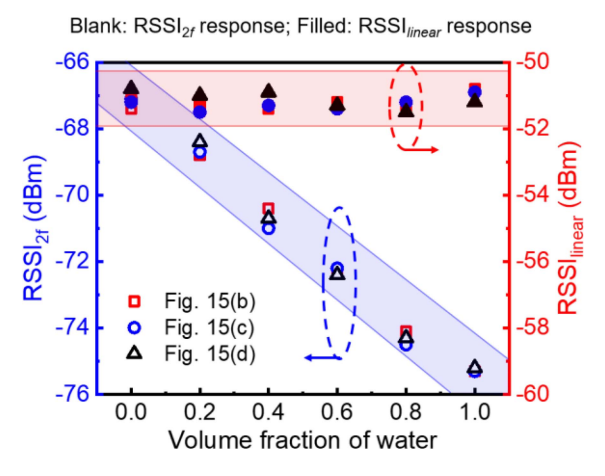
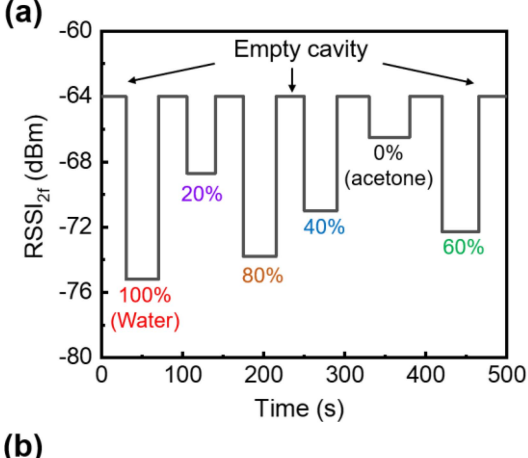


Fig. 16. The measured received signal strength indicator (RSSI) of the harmonic sensor (blue zone) and the conventional passive backscatter sensor (red zone).

the distance between T_x and the harmonic sensor, R_2 is the distance between R_x and the harmonic sensor (Fig. 15(a)), L_{sys} is the system loss including the various losses due primarily to conversion loss of frequency doubler, return/insertion losses of diplexer, and other factors. From Fig. 14, the results imply that the realized gain G_1 , associated with the signal strength of the received fundamental tone, is almost constant, whereas the realized gain G_2 , associated with the second harmonic retransmitted by the sensor, decreases linearly with reducing the acetone concentration. Such results suggest that the received signal strength indicator (RSSI) at the second-harmonic frequency gradually diminishes and ultimately vanishes when reducing the acetone concentration, as can be seen in Fig. 16. Here, important parameters are: $P_t = 25 \text{ dBm}, R_1 = R_2 = 1.2 \text{ m}, G_T = 17.5 \text{ dBi}$ at 2.86 GHz, $G_R = 19.5$ dBi at 5. 72 GHz and $L_{doubler}$ ~ 20 dB at the input power level of 0 dBm. For making a fair comparison, we also adopted the linear interrogation method (i.e., traditional passive backscatter wireless sensor) to read the same antenna sensor. In this case, the elliptical microstrip antenna in Fig. 9 is disconnected from the frequency conversion device. The measured backscattered RF signal at 5.72 GHz is also presented in Fig. 16, where $RSSI_{2f}$ (blue) and RSSI_{linear} (red) represent the RSSI data at 5.72 GHz for the harmonic sensor and the linear one, respectively. It is obvious that in the linear interrogation scheme (without additional frequency upconversion), although the antenna's resonance is still modulated by the liquid type, the measured backscattering responses can hardly reveal changes in dielectric property, due to the electromagnetic interferences sourced from clutters and crosstalks between T_x and R_x antennas. As a result, a passive harmonic sensor based on the proposed dual-resonance, dualpolarization microstrip antennas can provide a more robust and reliable far field sensing performance in all scenarios. compared with conventional linear backscatter sensors/tags. We should emphasize that the application of this harmonic sensor is not limited to sensing acetone/water mixtures, but can be generalized to identification of any type of aqueous solution/mixture (e.g., ethanol, glucose, oil, etc) in chemical,



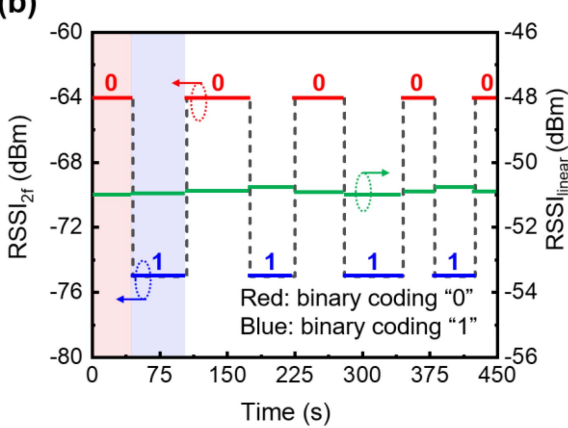


Fig. 17. Real time measurement results of the passive harmonic sensor with (a) different acetone-water mixture for real time wireless sensing, and (b) only water solution for binary "0" (empty) and "1" (100 % water) testing.

biological and environmental monitoring systems. The interrogating distance can be further increased by utilizing an active frequency doubler with a conversion gain [48].

Here, we also validate repeatability and continuity of our platform by performing the real-time measurement in the noisy environment. In our measurements, different concentrations of acetone-water mixture were injected in the fluidic channel every 80 seconds, with an interval of 20 seconds for the empty state reference. These experimental results shown in Fig. 17(a) demonstrate that a good sensitivity and robustness, as well as the capacity to conduct real-time wireless sensing (e.g., the lab-on-chip real-time parameter monitoring and detection). It is also seen from Fig. 17(a) that after injection of different acetone-water mixtures, the amplitudemodulated harmonic sensor can always be reset to its original state with a peak RSSI of -64 dBm. In Fig. 17(b), the purewater solution was injected in the sensor with random time intervals, showing that the existence of solution can effectively modulate the RSSI ("0" and "1") received in the far zone, whereas the conventional backscatter sensor fails to elaborate. We should also note that the proposed elliptical microstrip antenna could be integrated with more complicated microfluidic-channel networks on the same substrate and can be further miniaturized by using coplanar diplexer and frequency doubler.

V. CONCLUSION

We have proposed a compact, low-profile microstrip antenna for harmonic transponder sensors that demand a dual resonance at the fundamental and second-harmonic frequencies $(f_0 \text{ and } 2f_0)$. Specifically, we have investigated an elliptical patch antenna loaded with shorting pins, which can exhibit the TM_{e110} resonant mode at f_0 and the TM_{o110} resonant mode at $2f_0$, without coupling to other higher-order modes. Besides, these two modes have orthogonal linear polarizations, which further minimizes the background noises. Based on the perturbation theory, we have developed and tested a harmonic-based liquid sensor comprising the proposed dual-resonance, dual-polarization microstrip antenna integrated with a fluidic channel. We have demonstrated that such a nonlinear passive wireless sensor can successfully monitor the density of acetone-water mixtures, without being affected by multiple scattering coming from the ground or other objects (clutters). The compact, dualresonance microstrip antenna and its use for the development of zero-power, clutter-free harmonic-based liquid sensor show great potential in the remote sensing of humidity, moisture and other physiological factors, which have diverse industrial, environmental and wearable healthcare applications.

REFERENCES

- J. Zhang, G. Y. Tian, A. M. J. Marindra, A. I. Sunny, and A. B. Zhao, "A review of passive RFID tag antenna-based sensors and systems for structural health monitoring Applications," *Sensors*, vol. 17, no. 2, p. 265, 2017
- [2] X. Jia, Q. Feng, T. Fan, and Q. Lei, "RFID technology and its applications in Internet of Things (IoT)," in *Proc. 2nd Int. Conf. Consum. Electron Commun. Netw.*, 2012, pp. 1282–1285.
- [3] S. Z. Chen, H. Xu, D. Liu, B. Hu, and H. C. Wang, "A vision of IoT: Applications, challenges, and opportunities with China perspective," *IEEE Internet Things J.*, vol. 1, no. 4, pp. 349–359, Aug. 2014.
- [4] A. Vena, L. Sydanheimo, M. M. Tentzeris, and L. Ukkonen, "A fully inkjet-printed wireless and chipless sensor for CO₂ and temperature detection," *IEEE Sensors J.*, vol. 15, no. 1, pp. 89–99, Jan. 2015.
- [5] L. Yang, R. Zhang, D. Staiculescu, C. P. Wong, and M. M. Tentzeris, "A novel conformal RFID-enabled module utilizing inkjet-printed antennas and carbon nanotubes for gas-detection applications," *IEEE Antennas Wireless Propag. Lett.*, vol. 8, pp. 653–656, 2009.
- [6] B. S. Cook, J. R. Cooper, and M. M. Tentzeris, "An inkjet-printed microfluidic RFID-enabled platform for wireless lab-on-chip applications," *IEEE Trans. Microw. Theory Techn.*, vol. 61, no. 12, pp. 4714–4723, Dec. 2013.
- [7] W. Su, B. S. Cook, Y. Fang, and M. M. Tentzeris, "Fully inkjet-printed microfluidics: A solution to low-cost rapid three-dimensional microfluidics fabrication with numerous electrical and sensing applications," *Sci. Rep.*, vol. 6, Oct. 2016, Art. no. 35111.
- [8] P.-Y. Chen, H. Huang, and C.-H. Hung, "Compact metamaterial-enclosed wireless sensors with subtle perception of internal physical events," *Appl. Phys. Lett.*, vol. 107, no. 19, 2015, Art. no. 194101.
- [9] P.-Y. Chen et al., "Generalized parity-time symmetry condition for enhanced sensor telemetry," Nat. Electron., vol. 1, no. 5, pp. 297–304, May 2018.
- [10] M. Hajizadegan, M. Sakhdari, S. Liao, and P.-Y. Chen, "High-sensitivity wireless displacement sensing enabled by PT-symmetric telemetry," *IEEE Trans. Antennas Propag.*, vol. 67, no. 5, pp. 3435–3449, May 2019.
- [11] J. R. Riley et al., "Tracking bees with harmonic radar," Nature, vol. 379, pp. 29–30, Jan. 1996.
- [12] H. Y. Huang et al., "Chemical-sensitive graphene modulator with a memory effect for Internet-of-things applications," Microsyst. Nanoeng., vol. 2, May 2016, Art. no. 16018.

- [13] H. Y. Huang, M. Sakhdari, M. Hajizadegan, A. Shahini, D. Akinwande, and P.-Y. Chen, "Toward transparent and self-activated graphene harmonic transponder sensors," *Appl. Phys. Lett.*, vol. 108, no. 17, 2016, Art. no. 173503.
- [14] M. Hajizadegan et al., "Graphene sensing modulator: Toward low-noise, self-powered wireless microsensors," *IEEE Sensors J.*, vol. 17, no. 22, pp. 7239–7247, Nov. 2017.
- [15] S. Kim et al., "A novel dual-band retro-directive reflector array on paper utilizing substrate integrated waveguide (SIW) and inkjet printing technologies for chipless RFID tag and sensor applications," in MTT-S Int. IEEE Microw. Symp. Dig., Seattle, WA, USA, Jun. 2013, pp. 1–4.
- [16] S. Bouaziz, F. Chebila, A. Traille, P. Pons, H. Aubert, and M. M. Tentzeris, "Novel microfluidic structures for wireless passive temperature telemetry medical systems using radar interrogation techniques in Ka-band," *IEEE Antennas Wireless Propag. Lett.*, vol. 11, pp. 1706–1709, 2012.
- [17] B. S. Cook et al., "RFID-based sensors for zero-power autonomous wireless sensor networks," *IEEE Sensors J.*, vol. 14, no. 8, pp. 2419–2431, Aug. 2014
- [18] X. Gu, N. N. Srinaga, L. Guo, S. Hemour, and K. Wu, "Diplexer-based fully passive harmonic transponder for sub-6-GHz 5G-compatible IoT applications," *IEEE Trans. Microw. Theory Tech.*, vol. 67, no. 5, pp. 1675–1687, May 2019.
- [19] K. Rasilainen, J. Ilvonen, J.-M. Hannula, and V. Viikari, "Designing harmonic transponders using lumped-component matching circuits," *IEEE Antennas Wireless Propag. Lett.*, vol. 16, pp. 246–249, 2017.
- [20] V. Palazzi, F. Alimenti, C. Kalialakis, P. Mezzanotte, A. Georgiadis, and L. Roselli, "Highly integrable paper-based harmonic transponder for low-power and long-range IoT applications," *IEEE Antennas Wireless Propag. Lett.*, vol. 16, pp. 3196–3199, 2017.
- [21] X. Gu, L. Guo, S. Hemour, and K. Wu, "Analysis and exploitation of diplexer-based fully passive harmonic transponder for 5G applications," in *Proc. IEEE MTT-S Int. Microw. Workshop Series 5G Hardw. Syst. Technol.*, Dublin, Ireland, Aug. 2018, pp. 1–3.
- [22] H. Huang, P.-Y. Chen, C.-H. Hung, R. Gharpurey, and D. Akinwande, "A zero power harmonic transponder sensor for ubiquitous wireless μL liquid-volume monitoring," Sci. Rep., vol. 6, JAn. 2016, Art. no. 18795.
- [23] L. Zhu, N. Alkhaldi, H. M. Kadry, S. L. Liao, and P.-Y. Chen, "A compact hybrid-fed microstrip antenna for harmonics-based radar and sensor systems," *IEEE Antennas Wireless Propag. Lett.*, vol. 17, pp. 2444–2448, 2018.
- [24] D. Ahbe, S. Beer, T. Zwick, Y. Wang, and M. M. Tentzeris, "Dual-band antennas for frequency-doubler-based wireless strain sensing," *IEEE Antennas Wireless Propag. Lett.*, vol. 11, pp. 216–219, 2012.
- [25] K. R. Carver and J. W. Min, "Microstrip antenna technology," *IEEE Trans. Antennas Propag.*, vol. 29, no. 1, pp. 2–24, Jan. 1981.
- [26] W. F. Richards, Y. T. Lo, and D. D. Harriso, "An improved theory for microstrip antennas and applications," *IEEE Trans. Antennas Propag.*, vol. 29, no. 1, pp. 34–46, Jan. 1981.
- [27] P. Y. Chen and A. Alu, "Dual-mode miniaturized elliptical patch antenna with μ-negative metamaterials," *IEEE Antennas Wireless Propag. Lett.*, vol. 9, pp. 351–354, 2010.
- [28] P. Y. Chen and A. Alu, "Sub-wavelength elliptical patch antenna loaded with μ-negative metamaterials," *IEEE Trans. Antennas Propag.*, vol. 58, no. 9, pp. 2909–2919, Sep. 2010.
- [29] J. C. Gutiérrez-Vega, R. M. Rodriguez-Dagnino, M. A. Meneses-Nava, and S. Chávez-Cerda, "Mathieu functions, a visual approach," *Amer. J. Phys.*, vol. 71, no. 3, pp. 233–242, 2003.
- [30] D. A. Goldberg, L. J. Laslett, and R. A. Rimmer, "Modes of elliptical waveguides: A correction," *IEEE Trans. Microw. Theory Tech.*, vol. 38, no. 11, pp. 1603–1608, Nov. 1990.
- [31] ANSYS 2020 R1 Academic Research Electromagnetics Suite, Released in 2020, ANSYS Inc., Canonsburg, PA, USA, 2020.
- [32] D. R. Jackson, "Introduction to microstrip antennas," in *Proc. IEEE Int. Symp. Antennas Propag. USNC URSI Nat. Radio Sci. Meeting*, Orlando, FL, USA, 2013, pp. 1–179.
- [33] D. C. Nascimento and J. C. da S. Lacava, "Design of low-cost probe-fed microstrip antennas," in *Microstrip Antennas*, Nasimuddin, Eds. Rijeka, Croatia: InTech, 2011, pp. 1–26.
- [34] S. S. Zhong and Y. T. Lo, "Single-element rectangular microstrip antenna for dual-frequency operation," *Electron. Lett.*, vol. 19, no. 8, pp. 298–300, 1983.
- [35] R. B. Waterhouse and N. V. Shuley, "Dual frequency microstrip rectangular patches," *Electron. Lett.*, vol. 28, no. 7, pp. 606–607, 1992.
- [36] D. Schaubert, F. G. Farrar, A. Sindoris, and S. T. Hayes, "Microstrip antennas with frequency agility and polarization diversity," *IEEE Trans. Antennas Propag.*, vol. 29, no. 1, pp. 118–123, Jan. 1981.

- [37] H. K. Kan and R. B. Waterhouse, "Size reduction technique for shorted patches," *Electron. Lett.*, vol. 35, no. 12, pp. 948–949, 1999.
- [38] R. B. Waterhouse, S. D. Targonski, and D. M. Kokotoff, "Design and performance of small printed antennas," *IEEE Trans. Antennas Propag.*, vol. 46, no. 11, pp. 1629–1633, Nov. 1998.
- [39] X. Zhang and L. Zhu, "Patch antennas with loading of a pair of shorting pins toward flexible impedance matching and low cross polarization," *IEEE Trans. Antennas Propag.*, vol. 64, no. 4, pp. 1226–1233, Apr. 2016.
- [40] C. Gao, T. Wei, F. Duewer, Y. Lu, and X.-D. Xiang, "High spatial resolution quantitative microwave impedance microscopy by a scanning tip microwave near-field microscope," *Appl. Phys. Lett.*, vol. 71, no. 13, pp. 1872–1874, 1997.
- [41] H. Huang et al., "RFID tag helix antenna sensors for wireless drug dosage monitoring," IEEE J. Transl. Eng. Health Med., vol. 2, no. 1700108, pp. 1–8, Mar. 2014.
- [42] K. Saeed, R. D. Pollard, and I. C. Hunter, "Substrate integrated waveguide cavity resonators for complex permittivity characterization of materials," *IEEE Trans. Microw. Theory Tech.*, vol. 56, no. 10, pp. 2340–2347, Oct. 2008.
- [43] C. G. Malmberg and A. A. Maryott, "Dielectric constant of water from 0° to 100°C," J. Res. Nat. Bureau Standards, vol. 56, no. 1, pp. 1–8, 1956.
- [44] G. Akerlof, "Dielectric constants of some organic solvent-water mixtures at various temperatures," *J. Amer. Chem. Soc.*, vol. 54, no. 11, pp. 4125–4139, 1932.
- [45] Connectorized Diplexer ZDSS-3G4G-S+ From Mini-Circuit. Accessed: Jan. 14, 2019. [Online]. Available: https://www.minicircuits.com/ WebStore/dashboard.html?model=ZDSS-3G4G-S%2B
- [46] MULTIPLIER ZX90-2-36-S+ From Mini-Circuit. Accessed: Jan. 14, 2019. [Online]. Available: https://www.minicircuits.com/ WebStore/dashboard.html?model=ZX90Ű2-36-S%2B
- [47] J. A. Shaw, "Radiometry and the Friis transmission equation," Amer. J. Phys., vol. 81, no. 1, pp. 33–37, 2013.
- [48] F. Amato and S. Hemour, "The harmonic tunneling tag: A dual-band approach to backscattering communications," in *Proc. IEEE Int. Conf.* RFID Technol. Appl. (RFID TA), Pisa, Italy, 2019, pp. 244–247.



Liang Zhu (Graduate Student Member, IEEE) received the M.Sc. degree in optics from Sun Yat-Sen University, Guangzhou, China, in 2015. He is currently pursuing the Ph.D. degree in electrical engineering with the University of Illinois, Chicago. His research mainly focuses on RF/microwave antennas and circuits, energy harvesting platforms, and wireless sensors.



Nabeel Alsaab received the B.S. degree in electrical engineering from Purdue University, Indiana, and the first master's degree in electrical engineering from Wayne State University, Detroit, in 2017, and the master's degree in engineering systems management from St. Mary's University, San Antonio, in 2011. He is currently pursuing the Ph.D. degree in electrical engineering with the University of Illinois, Chicago. He is a Lecturer with the Department of Electrical Engineering, Qassim University, Saudi Arabia. In 2012, he was an Operation Manager with

KACST Solar Village/PV Module Assembly Line, Saudi Arabia. His research interest lies in the area of design a smart sensors and wireless communication.



Mark Ming-Cheng Cheng (Member, IEEE) received the B.S. and Ph.D. degrees from National Tsing-Hua University, Taiwan, in 1995 and 2003, respectively. He is a Professor with the Department of Electrical and Computer Engineering, University of Alabama, Tuscaloosa, where he joined in 2019. He was a NIH Postdoctoral Fellow with the Heart and Lung Research Institute, Ohio State University, Columbus, from 2003 to 2005, and was a Research Assistant Professor with the Department of Nanomedicine and Biomedical Engineering,

University of Texas Health Science Center, Houston, from 2006 to 2007. From 2008 to 2018, he went through the academic ranks to a Full Professor with the Department of Electrical and Computer Engineering and Biomedical Engineering, Wayne State University, Detroit, where he initialized curriculum in nanoengineering and cyber-physical systems. He has published approximate 120 papers in peer-review journal and conference proceedings. He has been involved in multidisciplinary research in microsystem design, biomedical devices, biosensors, new materials, wearable sensors, and environmental Internet-of-Things. He was recipient of the National Science (NSF) CAREER Award, the ONR Summer Faculty Fellowship, and the President Research Enhancement Award.



Pai-Yen Chen (Senior Member, IEEE) received the Ph.D. degree from the University of Texas at Austin in 2013. He is an Associate Professor with the Department of Electrical and Computer Engineering, University of Illinois, Chicago. He was a Research Scientist with Intellectual Ventures' Metamaterial Commercialization Center from 2013 to 2014, and a Research Staff with the National Nano Device Laboratory, Taiwan, from 2006 to 2009. He has published approximately 95 peer-review papers, 100 conference proceedings, one book, eight book

chapters, and 10 U.S. patents. He has been involved in multidisciplinary research on applied electromagnetics, wireless micro/nano-sensors and integrated systems, innovative RF antennas and circuits, metamaterials, and nano-electromagnetism in plasmonics and nanophotonics. He was a recipient of the National Science Foundation (NSF) CAREER Award; the IEEE Sensors Council Young Professional Award; the IEEE Raj Mittra Travel Grant Award; the SPIE Rising Researcher Award; the ACES Early Career Award; the Young Scientist Awards from PIERS; the URSI General Assembly and the URSI Commission B: Electromagnetics; the Air Force Research Laboratory Faculty Fellowship; the College of Engineering Faculty Research Excellence Award; the Donald Harrington Fellowship; the University of Texas Professional Development Award; the Taiwan Ministry of Education Study Abroad Award; the United Microelectronics Corporation Scholarship; and quite a few student paper awards and travel grants from major IEEE conferences, including the USNC-URSI Ernest K. Smith Student Paper Award. He currently serves as Associate Editor for IEEE SENSORS JOURNAL, the IEEE JOURNAL OF RADIO FREQUENCY IDENTIFICATION, the IEEE JOURNAL OF ELECTROMAGNETICS, RF AND MICROWAVES IN MEDICINE AND BIOLOGY, and a guest editor for several international journals. He was a former Associate Editor of Applied Electromagnetics.